Research Article Vol. 34, No. 4 / 23 Feb 2026 / Optics Express 5801
Optics EXPRESS

Low-loss AlN films grown on sapphire by high-temperature MOCVD

HAIPENG LIU,[1,2] TIANYU SUN,[2,4] ANWEI ZHOU,[2,3] RUIGONG SU,[2] ZHENG XING,[2] JIJUN FENG,[1,5] ZHONGMING ZENG,[2] AND BAOSHUN ZHANG[2]

[1]*Shanghai Key Laboratory of Modern Optical System, Engineering Research Center of Optical Instrument and System (Ministry of Education), School of Optical-Electrical and Computer Engineering, University of Shanghai for Science and Technology, Shanghai 200093, China*
[2]*Nanofabrication Facility, Suzhou Institute of Nano-Tech and Nano-Bionics, Chinese Academy of Sciences, Suzhou 215123, China*
[3]*State Key Laboratory on High Power Semiconductor Lasers, Changchun University of Science and Technology, Changchun 130000, China*
[4]*tianyu.sun@hotmail.com*
[5]*fjijun@usst.edu.cn*

Abstract: Single-crystal AlN-on-sapphire, possessing both a strong Kerr nonlinear effect and high-power handling as well as a very large band gap, is a fascinating platform for integrated optics. High-temperature metal-organic chemical vapor deposition of AlN films is attractive as an elevated temperature is believed to enhance both the crystalline quality and the deposition efficiency. In this contribution, we report the epitaxy and characterization of AlN-on-sapphire grown at 1400°C. The AlN films had much improved crystalline quality in terms of the dislocation density, XRD FWHM values, and AFM root-mean-square roughness. A fully etched MRR was fabricated with the standard i-line photolithography, and an intrinsic Q-factor of 5.1×10^6 is achieved at the wavelength of 1553 nm in the TE polarization, indicating a low propagation loss of less than 0.073 dB/cm. Furthermore, efficient thermo-optic tuning was demonstrated with an integrated thermal heater, delivering a tuning efficiency of 0.65 pm/mW across one FSR while maintaining a high Q-factor above 4.1×10^6.

© 2026 Optica Publishing Group under the terms of the Optica Open Access Publishing Agreement

1. Introduction

AlN is a promising material for integrated photonics due to its attractive optical properties, including transparency down to deep UV wavelengths [1], strong Pockels effect [2,3], significant second-order and third-order optical nonlinearity as well as high thermal conductivity [4,5]. AlN-on-sapphire platform shows promises for large scale integrated photonics at infrared (1550 nm), near-infrared (NIR) (780 nm), and ultraviolet (396 nm). By leveraging the high-power handling of AlN waveguide and the relatively high thermal conductivity of sapphire substrate, AlN-on-sapphire platform enables integrated photonic devices operating at high laser powers [6,7]. Realizing low loss waveguides and high-Q micro-ring resonators (MRRs) on AlN-on-sapphire platform can pave the way for on-chip nonlinear photonic and quantum photonic devices [8–10].

The realization of low loss waveguides and high-quality factor MRRs has been limited by AlN material quality, the surface and sidewall roughness induced either during epitaxy or fabrication process. Due to the large lattice mismatch, AlN grown on sapphire generally has dislocation densities of $10^9\,\mathrm{cm}^{-2}$ or higher [11]. This internal defect induced scattering loss is strongly dependent on polarization and waveguide geometries. The large core waveguide exhibits strongest performance dependence on material crystalline quality [12]. Furthermore, according to the Rayleigh formula, the scattering cross-section is proportional to λ^{-4}, indicating

#584469 https://doi.org/10.1364/OE.584469
Journal © 2026 Received 11 Nov 2025; revised 15 Jan 2026; accepted 26 Jan 2026; published 9 Feb 2026

Optics EXPRESS

that crystalline defects will cause higher scattering loss in ultraviolet-visible wavelengths than in infrared wavelengths.

High-temperature (HT) MOCVD is one of the best methods to reduce not only the number of dislocations but also the content of the impurities and point defects [13,14]. At high growth temperature, AlN films can achieve high surface growth rate, and the resultant AlN crystal surface is atomically flat [15]. Imura and co-workers reported high quality AlN layers grown on 6H-SiC substrates at temperatures as high as 1600°C [16]. Chen et al. obtained high quality AlN-on-sapphire by optimizing the growth temperature of AlN nucleation layer using HT MOCVD [17]. An et al. investigated the process parameters using an optimized multi-physical field numerical model and concluded that a HT environment is necessary to promote surface diffusion of Al atoms and Al free radicals [18].

In this paper, we present an AlN epitaxial layer grown on sapphire by HT MOCVD and the fabrication of low loss waveguides and high-Q MRRs. We achieved high crystalline quality AlN films. With the standard i-line photolithography technique, an intrinsic Q-factor of 5.1×10^6 was demonstrated at the wavelength of 1553 nm, corresponding to 0.073 dB/cm propagation loss. Efficient thermo-optic tuning was further demonstrated with a linear response of 0.65 pm/mW, while maintaining a high intrinsic Q-factor above 4.1×10^6 over a resonance shift of one FSR.

2. AlN film preparation and characterization

AlN films were grown using Taiyo Nippon Sanso MOCVD platform on a 2-inch *c*-plane (0001) sapphire substrate, with a miscut of 0.2° toward the *m*-axis. Trimethyl-aluminum (TMAl) and ammonia (NH_3) were used as precursors. Prior to growth, thermal cleaning of the substrate was carried out for 5 minutes in hydrogen ambience at 1130°C in order to promote the desorption of oxygen atoms on the surface [19,20]. A 20-nm-thick low-temperature (LT) AlN buffer layer was first deposited in a continuous gas flow mode at 600°C with a V/III ratio of 3000. Then, 500 nm AlN was epitaxially grown at 1400°C with a V/III ratio of 268. For reference, 500-nm AlN films were also grown at 1175°C with a V/III ratio of 1225.

An 18-point thickness measurement on our AlN samples yielded an average thickness of 505.67 nm. The refractive index measured by ellipsometry was 2.02 at 1550 nm. X-ray diffraction (XRD) was used to assess the crystal quality of the AlN films, as shown in Fig. 1. The full-width at half-maximum (FWHM) values of the symmetric (0002) X-ray rocking curves for AlN grown at temperatures of 1175°C and 1400°C were 41 and 23 arcseconds, respectively. The FWHM values of the asymmetric $(10\bar{1}2)$ X-ray rocking curves were 980 and 330 arcseconds, respectively. High-temperature growth promotes grain growth, thus improves the crystalline quality of AlN films [21].

As scattering loss induced by internal defects is critical to waveguide performance [12], we employ transmission electron microscopy (TEM) to analyze crystalline defects at the microscale. Dislocation densities were quantified using plan-view TEM images. Figure 2(a) presents a bright-field plan-view TEM image of the AlN layer grown at 1175 °C. Dislocations appearing as single lines correspond to edge-type dislocations, while those composed of lines and pairs represent mixed-type dislocations, spot-like features are attributed to screw-type dislocations. These dislocations primarily originate from small-angle grain boundaries [20]. For the AlN layer grown at 1175°C, the estimated densities of edge, screw, and mixed dislocations are 6.8×10^9, 8×10^8, and $8.6 \times 10^9\,\mathrm{cm}^{-2}$, respectively. Figures 2(b)-(c) show bright-field plan-view TEM images of the AlN layer grown at 1400°C. From plan-view TEM analysis, the edge, screw, and mixed dislocation densities are determined to be 3×10^8, 1×10^7, and $1.5 \times 10^8\,\mathrm{cm}^{-2}$, respectively. Figures 2(d)-(f) also show bright-field cross-sectional TEM images of AlN layers grown at 1400 °C. Notably, FWHM values of symmetric diffractions have been correlated with screw and mixed dislocation densities, whereas FWHM values of asymmetric diffractions correlate with edge and mixed dislocation densities [20]. Overall, the dislocation density of AlN films grown at

Optics EXPRESS

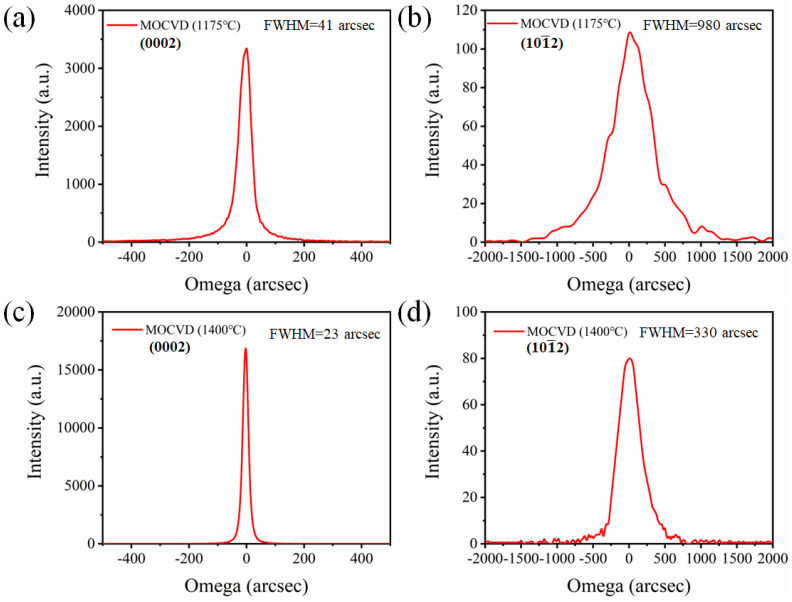

Fig. 1. XRD rocking curves of the (0002) and (10$\bar{1}$2) planes of AlN films grown at 1175°C and 1400°C, respectively.

1400°C is one order of magnitude lower than that grown at 1175°C. Edge-type dislocations, assumed to significantly contribute to scattering losses in AlN waveguides and primarily caused by small-angle grain boundaries [20], predominate under low-growth-temperature conditions. In contrast, edge dislocation densities decrease substantially with increasing growth temperature, accompanied by the formation of larger grains. These results demonstrate that HT growth yields AlN films with superior crystalline quality, lower defect densities, and consequently reduced scattering losses in AlN waveguides.

The AlN film surface morphologies, including grain size, step-flow growth features, and surface defect density (e.g., pits and protrusions), were evaluated by atomic force microscopy (AFM) over a $5 \times 5\ \mu m^2$ area. Figure 3 shows the AlN films grown at 1175°C, with root mean square (RMS) roughness values of 0.412 nm and 0.477 nm at the center and the edge, respectively. The surface of AlN film at low temperature appears step-like. With increasing growth temperature, smaller grains are incorporated into bigger grains and the surface morphology improved and became atomically flat. The roughness of the AlN film grown at 1400°C was as low as 0.105 nm and 0.132 nm at the center and the edge. High temperature promotes the reorganization of surface atoms, forming a smoother step-flow surface and reducing roughness caused by island growth. Additionally, high temperature facilitates the volatilization of impurities adsorbed on the surface (such as carbon and oxygen), thereby improving the film's purity [22,23].

3. Fabrication and characterization of micro-ring resonators

To verify high crystalline quality of the HT MOCVD-grown AlN film, a 500 nm thick AlN MRR was fabricated and covered with a 1.0 µm SiO_2 layer, as shown in Fig. 4. The MRR uses a pulley coupling structure, which is highly tolerant to gap variations within the coupling region. The pulley angle was set from 70° to 160° to meet under-coupling, critical coupling, and over-coupling conditions. The inner ring has a radius of 480 µm and a width of 1.04 µm, while the outer ring has a radius of 481.62 µm and a width of 1.0 µm. The coupling gap is 700 nm. The

Optics EXPRESS

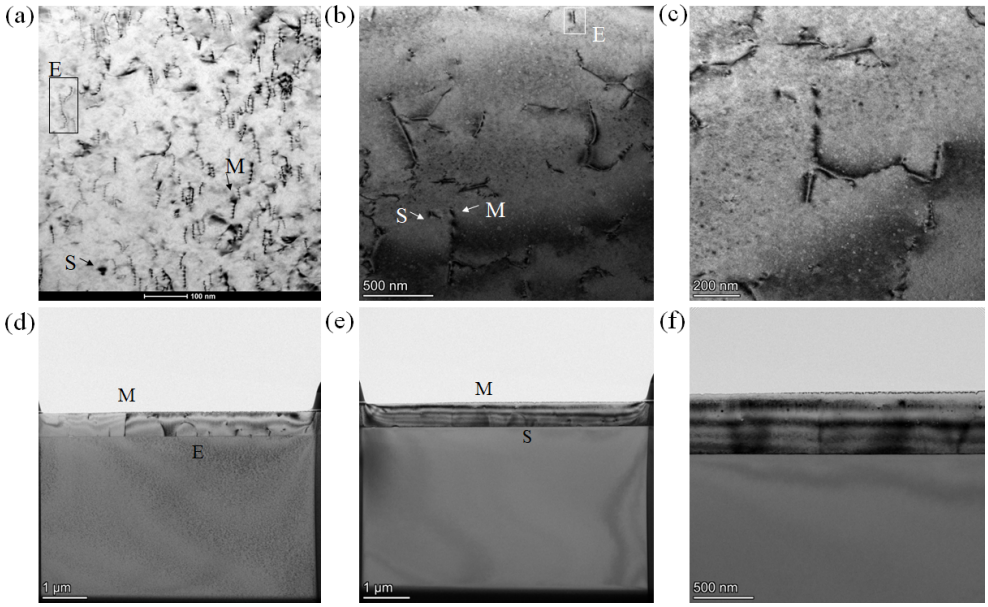

Fig. 2. Tilted 8° from the (0001) zone axis taken under two-beam conditions with $\boldsymbol{g} = [11\bar{2}0]$. Bright-field plan-view TEM images of AlN film grown at (a) 1175°C and (b)-(c) 1400°C, respectively. Bright-field cross-sectional TEM images of AlN layer grown at 1400°C taken under different two-beam conditions with (d) $\boldsymbol{g} = [0002]$ and (e)-(f) $\boldsymbol{g} = [11\bar{2}0]$.

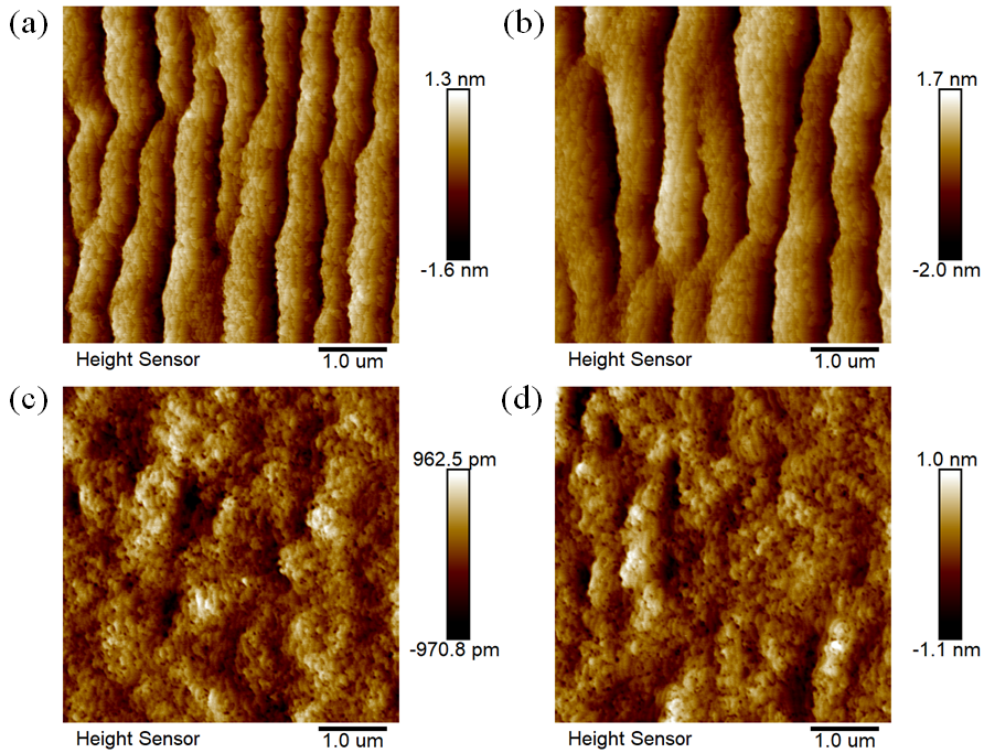

Fig. 3. AFM images of the (a) center and (b) edge of an AlN film grown at 1175°C. AFM images of the (c) center and (d) edge of an AlN film grown at 1400°C.

Optics EXPRESS

bus waveguide is 1.0 µm wide, that ensures single-mode operation over range of 1500 to 1600 nm. Adiabatically tapers are adopted at input/output ends.

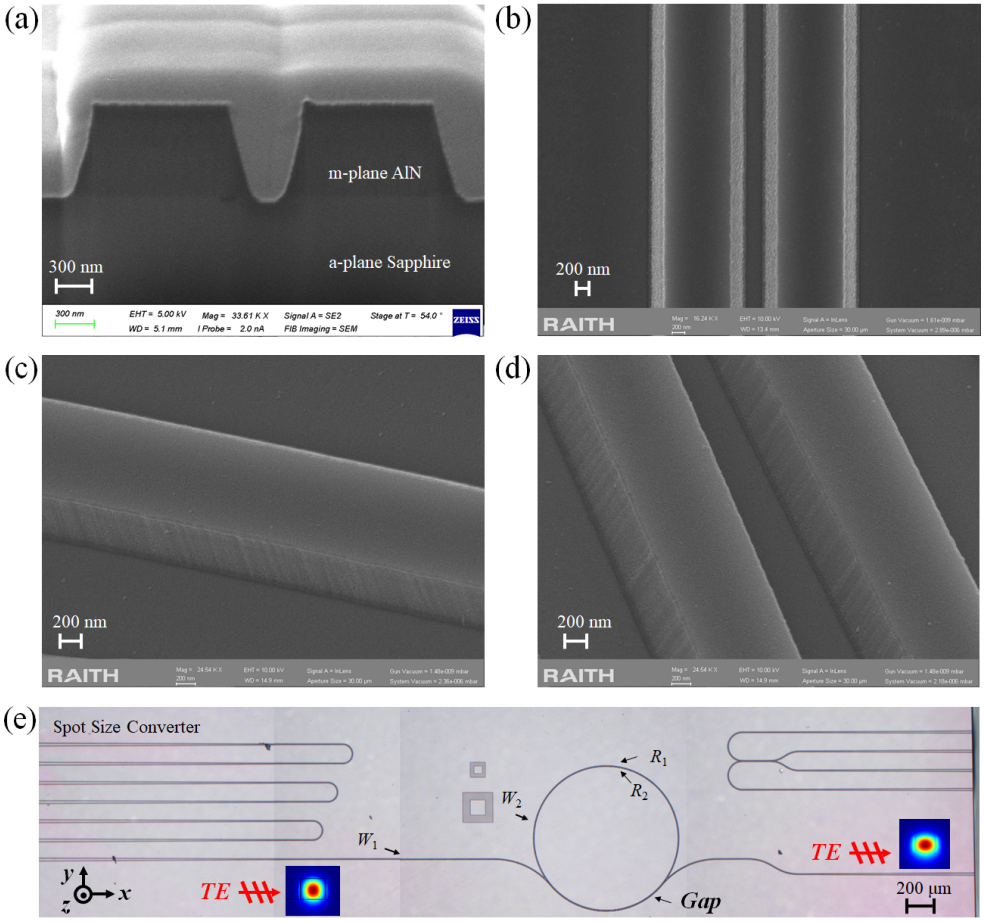

Fig. 4. (a) Cross-sectional SEM, (b)-(d) top view SEM, and (e) microscope images of the fabricated MRR.

For the MRR fabrication, a 1.0 µm SiO_2 mask was initially deposited using plasma-enhanced chemical vapor deposition (PECVD). The MRRs are defined using the Nikon I755I7B Stepper System based on i-line UV illumination. The photoresist pattern was transferred to the 1.0 µm SiO_2 hard mask via advanced oxide etching (AOE). The AlN was etched using $Cl_2/BCl_3/Ar$ gas mixture in an inductively coupled plasma (ICP) system (Naura). The flow rates for Cl_2, BCl_3, and Ar were set to 60, 5, and 10 sccm, respectively, with an ICP power of 250 W, a bias voltage of −200 V, and a chamber pressure of 8 mTorr. Figure 4 presents scanning electron microscope (SEM) top-view and cross-sectional images of the fabricated MRR respectively. The AlN waveguide exhibits a smooth surface and sharp, steep sidewalls, demonstrating the excellent directionality and effectiveness of the dry etching process. Finally, the MRRs were covered with 1.0 µm SiO_2 for test.

To characterize the fabricated MRRs, a tunable semiconductor laser (TSL-570, Santec) was used for sweeping with a step of 0.1 pm. A manual fiber polarization controller was inserted for polarization control and a multiport optical power meter (MPM 220, Santec) was utilized as

Optics EXPRESS

detector. The laser power was set to 0 dBm. The tuning and recording interval of the tunable laser and optical power meter are both 100 ms.

Figure 5(a) and (c) show the transmission spectra of AlN MRRs grown at 1175°C and 1400°C in the TE polarization, respectively. The excited mode experience under-coupling, critical coupling and over-coupling from 1540 nm to 1560 nm. The highest extinction ratio exceeding 20 dB indicates the near-critically coupling. The FSR was determined to be 0.39 nm, resulting in a group index (n_g) of the fundamental TE mode of 2.052. The loaded quality of MRRs is determined by the intrinsic quality factor and the coupling quality factor, as shown

$$Q_{int} = \frac{2\pi n_g}{\lambda \alpha} = \frac{2Q_{load}}{1 \pm \sqrt{T}} \tag{1}$$

$$\frac{1}{Q_{load}} = \frac{1}{Q_{int}} + \frac{1}{Q_C} \tag{2}$$

where λ, α, and n_g represent the wavelength, intrinsic loss, and group index, respectively, T denotes the normalized resonant transmittance value, while the coupling state determines its leading sign.

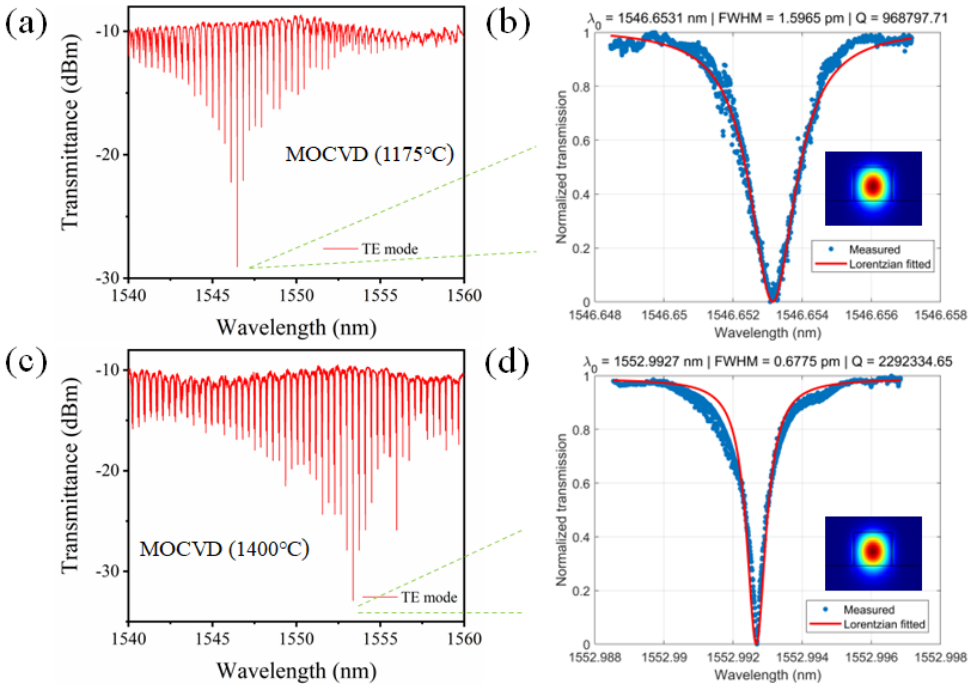

Fig. 5. Transmission spectra of the AlN MRR grown using MOCVD at 1175°C (a) and 1400°C (c), respectively. (b) and (d) are the Lorentzian fits and extracted Q factors of the corresponding resonant spectra.

Figure 5(b) and (d) display the Lorentzian fitting curves for the resonant linewidth of the MRR. The FWHMs are 1.59 pm and 0.67 nm, corresponding to the loaded quality factors of 9.68×10^5 and 2.29×10^6, respectively. The calculated intrinsic quality factors are 2.15×10^6 and 5.1×10^6, respectively, and the intracavity intrinsic losses are estimated to be 0.178 and 0.073 dB/cm.

Frequency stabilization based on the high-Q MRR shows promise for enabling ultra-narrow-linewidth laser emission. However, the challenge lies in maintaining low optical loss and high frequency stability. Considering that the dominant sources of frequency noise within dielectrics

Optics EXPRESS

is thermal refractive noise, resonators with small thermo-optic response are desirable for on-chip reference cavities. Therefore, we characterize the relationship of temperature-based resonance shift in the infrared band by applying a bias voltage to the microheater integrated on the MRR. For thermal micro heater, 150 nm NiCr was patterned on top of SiO_2 cladding of MRR using UV lithography, and Ti (10 nm)/Al (800 nm)/Au (90 nm) were evaporated as metal contact pads using photolithography [6]. Figure 6(a) shows the optical microscope image of the fabricated MRR with thermal heater. Figure 6(b) presents the transmission spectra of the thermal heater under different applied currents. When the current applied to the thermal phase shifter is swept from 0 to 200 mA, the resonant wavelength of the MRR red-shifts by 0.385 nm, which is close to one FSR. Figure 6(c) shows the Lorentzian fitting curves for the resonant linewidth of the MRR for different heater currents applied. The AlN-MRRs maintain a high intrinsic Q value, decreasing only from 4.61×10^6 to 4.1×10^6, corresponding to estimated intracavity intrinsic losses of 0.083 and 0.094 dB/cm. Figure 6(d) shows a clear linear relationship between the resonant frequency shift and the applied thermal power, with a slope of 0.65 pm/mW. Owing to the potential for very low propagation loss and precise thermal tunability, this waveguide platform represents a significant step toward realizing thermally stable integrated resonators for on-chip laser frequency stabilization and other applications.

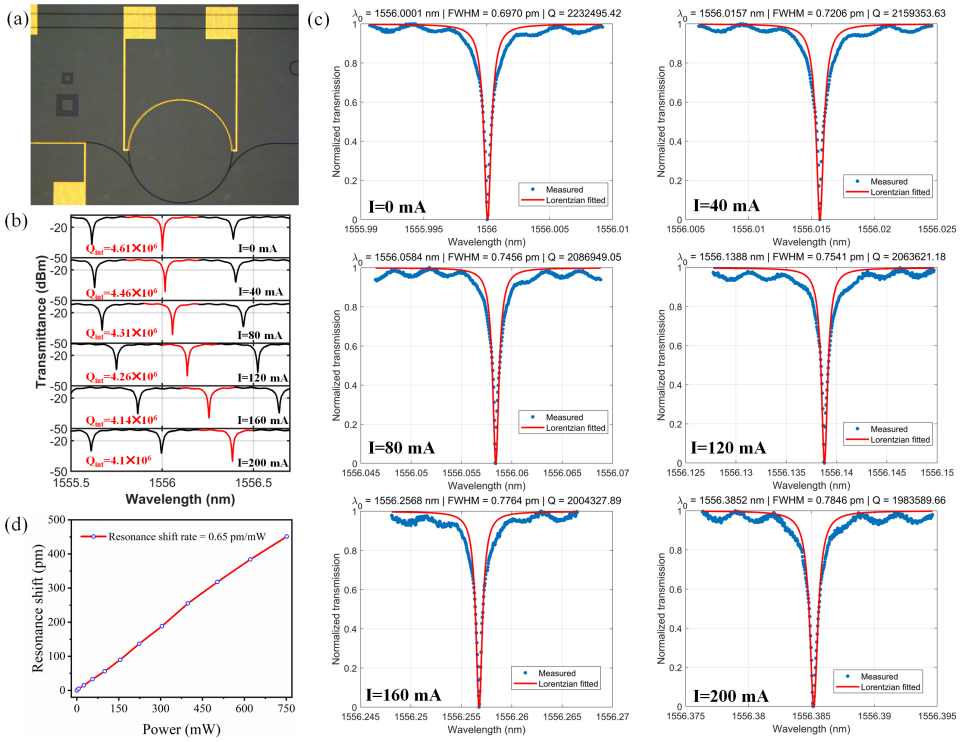

Fig. 6. (a) Microscope images of the micro-ring resonator electrode. (b) Resonator transmission curves used to extract the thermal shift. (c) The Lorentz fit curve of the resonant spectrum. (d) The transmission peak wavelength as a function of applied thermal heater power, giving the resonator thermo-optic shift.

4. Conclusion

In this paper, AlN films on sapphire grown at a temperature of 1400°C were demonstrated with improved crystalline quality in terms of the dislocation density, XRD FWHM values, and AFM

Optics EXPRESS

root-mean-square roughness. The dislocation density estimated from the plan-view TEM images was reduced to $1.5 \times 10^8\,\mathrm{cm}^{-2}$, thereby reducing scattering loss in the waveguide. Using the standard i-line lithography technology, we fabricated fully etched AlN MRRs and achieved intrinsic Q values of up to 5.1×10^6 at a wavelength of 1553 nm, corresponding to an intrinsic loss of 0.073 dB/cm. Furthermore, efficient thermo-optic tuning of the MRR was demonstrated, exhibiting a linear response of 0.65 pm/mW while maintaining a high intrinsic Q-value above 4.1×10^6 throughout one FSR. This low-loss AlN-on-sapphire platform is ideal for nonlinear photonic and quantum photonic chips.

Funding. National Key Research and Development Program of China (2022YFB2804601, 2022YFB2802500, 2022YFE0107400); National Natural Science Foundation of China (U23A20381); Science and Technology Commission of Shanghai Municipality (23010503600, 23530730500).

Disclosures. The authors declare no conflicts of interest.

Data availability. Data underlying the results presented in this paper are not publicly available at this time but may be obtained from the authors upon reasonable request.

References

1. N. Li, C. P. Ho, S. Zhu, *et al.*, "Aluminium nitride integrated photonics: a review," Nanophotonics **10**(9), 2347–2387 (2021).
2. S. X. Xue, M. X. Li, R. Lopez-rios, *et al.*, "Pockels laser directly driving ultrafast optical metrology," Light: Sci. Appl. **14**(1), 209 (2025).
3. M. X. Li, L. Chang, L. Wu, *et al.*, "Integrated Pockels laser," Nat. Commun. **13**(1), 5344 (2022).
4. X. W. Liu, C. Z. Sun, B. Xiong, *et al.*, "Aluminum nitride-on-sapphire platform for integrated high-Q microresonators," Opt. Express **25**(2), 587–594 (2017).
5. Y. L. Ding, Y. F. Wang, S. Y. Yao, *et al.*, "Self-Injection Locking Dynamics with Raman Actions in Aluminum Nitride Microresonators," Phys. Rev. Lett. **135**(9), 093801 (2025).
6. W. Shin, Y. Sun, M. Soltani, *et al.*, "Demonstration of green and UV wavelength high Q aluminum nitride on sapphire microring resonators integrated with microheaters," Appl. Phys. Lett. **118**(21), 211103 (2021).
7. K. Liu, Z. Wang, S. Yao, *et al.*, "Mitigating fast thermal instability by engineered laser sweep in AlN soliton microcomb generation," Photonics Res. **11**(8), A10–A18 (2023).
8. Y. He, R. Lopez-Rios, U. A. Javid, *et al.*, "High-speed tunable microwave-rate soliton microcomb," Nat. Commun. **14**(1), 3467 (2023).
9. T.-J. Lu, M. Fanto, H. Choi, *et al.*, "Aluminum nitride integrated photonics platform for the ultraviolet to visible spectrum," Opt. Express **26**(9), 11147–11160 (2018).
10. G. N. West, W. Loh, D. Kharas, *et al.*, "Low-loss integrated photonics for the blue and ultraviolet regime," APL. Photonics **4**(2), 026101 (2019).
11. Y. Sun, W. Shin, D. A. Laleyan, *et al.*, "Ultrahigh Q microring resonators using a single-crystal aluminum-nitride-on-sapphire platform," Opt. Lett. **44**(23), 5679–5682 (2019).
12. H. Chen, H. Fu, J. Zhou, *et al.*, "Study of crystalline defect induced optical scattering loss inside photonic waveguides in UV–visible spectral wavelengths using volume current method," Opt. Express **27**(12), 17262–17273 (2019).
13. H. Wu, Y. N. Guo, R. J. Zhang, *et al.*, "Simultaneous edge and surface stimulated emission from AlGaN-based deep ultraviolet laser bars," Opt. Express **33**(8), 17085–17093 (2025).
14. W. R. Song, X. F. Zhang, X. P. Zhou, *et al.*, "Low-threshold green lasing in heterogeneously integrated InGaN-based micro-rings covered by distributed Bragg reflectors on Si (100)," Opt. Express **32**(16), 27431–27443 (2024).
15. M. Imura, K. Nakano, T. Kitano, *et al.*, "Microstructure of thick AlN grown on sapphire by high-temperature MOVPE," Phys. Status. Solidi. A **203**(7), 1626–1631 (2006).
16. M. Imura, H. Sugimura, N. Fujimoto, *et al.*, "Impact of high-temperature growth by metal-organic vapor phase epitaxy on microstructure of AlN on 6H-SiC substrates," J. Crystal. Growth. **310**(7-9), 2308–2313 (2008).
17. Y. R. Chen, H. Song, D. B. Li, *et al.*, "Influence of the growth temperature of AlN nucleation layer on AlN template grown by high-temperature MOCVD," Mater. Lett. **114**(1), 26–28 (2014).
18. J. An, X. Y. Dai, L. S. Feng, *et al.*, "Parameter study of the high temperature MOCVD numerical model for AlN growth using orthogonal test design," Sci. Rep. **11**(1), 8877 (2021).
19. Y. Zhang, H. L. Long, J. Zhang, *et al.*, "Fast growth of high quality AlN films on sapphire using a dislocation filtering layer for ultraviolet light-emitting diodes," CrystEngComm **21**(27), 4072–4078 (2019).
20. M. Imura, K. Nakano, N. Fujimoto, *et al.*, "Dislocations in AlN epilayers grown on sapphire substrate by high-temperature metal-organic vapor phase epitaxy," Jpn. J. Appl. Phys. **46**(4R), 1458 (2007).
21. R. He, Y. X. Wang, Y. J. Song, *et al.*, "III-Nitride Micro-Array Integration for Photon Transceiver," Laser Photonics Rev. **20**(1), e00815 (2026).
22. Y. J. Song, R. He, J. X. Ran, *et al.*, "III-nitride-based monolithic integration: From electronics to photonics," Appl. Phys. Rev. **12**(2), 021301 (2025).
23. X. Y. Wu, J. J. Feng, X. T. Liu, *et al.*, "Effects of rapid thermal annealing on aluminum nitride waveguides," Opt. Mat. Express **10**(12), 3073–3080 (2020).